Discontinuous Galerkin methods for Numerical Weather Prediction

Giovanni Tumolo

giovanni.tumolo@ecmwf.int

European Centre for Medium-Range Weather Forecasts

This project has received funding from the European Union's Horizon 2020 research and innovation programme under grant agreement No 800987

DG pros and cons

- Discontinuous Galerkin (DG) methods for hyperbolic problems are
- appealing for:
  - high order accuracy,
  - great flexibility (non conforming meshes, polynomial order and even basis function type can vary elementwise),
  - good scalability (highly local),
- challenging for:
  - stability restrictions with explicit time stepping:

    "The RKDG algorithm is stable provided the following condition holds:

    $$u\frac{\Delta t}{h} < \frac{1}{2p+1}$$

    where p is the polynomial degree; (for the linear case this implies a CFL limit $\frac{1}{3}$)"

    Cockburn-Shu, Math. Comp. 1989

  - computational cost : DG requires more d.o.f. per element than CG .
- How to increase computational efficiency of DG for NWP applications?

DG for NWP: key points

What makes a DG code specifically designed for NWP different from a standard general porpuse DG code for CFD?

The choice of:

- time integrators;
- basis functions;
- adaptivity strategy;
- mesh;
- vertical coordinate;
- data structures;
- parallelization strategy;
- NO best choice available in absolute, I'll review SOME possible choices which make sense for NWP, more options are available!

Time integrators for NWP: the SISL technique

- "The“ time integration technique for grid point methods in NWP since seminal paper by Robert in 1981;

- The key idea: in the governing equations, terms responsible for fast waves propagation treated implicitly, while those responsible for slow waves (advection) treated explicitly, with the SL technique: unconditionally stable!

- Operational time integration approach for spectral transform dycore at ECMWF since 1991, used also by UM at UK Met Office, by Aladin - Hirlam and many others;

- To avoid any CFL condition, why not combine DG with the SI-SL technique?

Time integrators for NWP-DG models: a novel SISL approach

Given a Cauchy problem for a system of ODEs:

$$\begin{aligned}
\mathbf{y}' &= \mathbf{f}(\mathbf{y}, t), \qquad (1)\\
\mathbf{y}(0) &= \mathbf{y}_0,
\end{aligned}$$

the TR-BDF2 method is defined by the two following implicit stages (Bank et al. IEEE trans. 1985):

$$\begin{aligned}
\mathbf{u}^{n+2\gamma} - \gamma \Delta t \mathbf{f}(\mathbf{u}^{n+2\gamma}, t_n + 2\gamma\Delta t) &= \mathbf{u}^n + \gamma \Delta t \mathbf{f}(\mathbf{u}^n, t_n),\\
\mathbf{u}^{n+1} - \gamma_2 \Delta t \mathbf{f}(\mathbf{u}^{n+1}, t_{n+1}) &= (1-\gamma_3)\mathbf{u}^n + \gamma_3 \mathbf{u}^{n+2\gamma},
\end{aligned}$$

with $\gamma \in (0, 1/2]$ fixed implicitness parameter and

$$\gamma_2 = \frac{1-2\gamma}{2(1-\gamma)}, \quad \gamma_3 = \frac{1-\gamma_2}{2\gamma}.$$

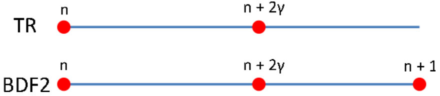

Time integrators for NWP-DG models: advantages of TR-BDF2

TR-BDF2, reformulated as a SDIRK method (Hosea Shampine ANM 1996),

$$
\begin{aligned}
\mathbf{k}_1 &= \mathbf{f}\left(\mathbf{u}^n, t_n\right), \\
\mathbf{k}_2 &= \mathbf{f}\left(\mathbf{u}^n + \gamma \Delta t \mathbf{k}_1 + \gamma \Delta t \mathbf{k}_2, t_n + \gamma \Delta t\right), \\
\mathbf{k}_3 &= \mathbf{f}\left(\mathbf{u}^n + \frac{1-\gamma}{2} \Delta t \mathbf{k}_1 + \frac{1-\gamma}{2} \Delta t \mathbf{k}_2 + \gamma \Delta t \mathbf{k}_3, t_{n+1}\right), \\
\mathbf{u}^{n+1} &= \mathbf{u}^n + \Delta t \left(\frac{1-\gamma}{2} \mathbf{k}_1 + \frac{1-\gamma}{2} \mathbf{k}_2 + \gamma \mathbf{k}_3\right),
\end{aligned}
$$

exhibits interesting properties like:

- it is L-stable;
- it is second order accurate but embedded in a third order companion (hence “free" asymptotically correct error estimate);
- all the stages are evaluated within the the step interval;
- it is First-Same-As-Least (FSAL), hence only two implicit stages to evaluate per step;

Time integrators for NWP-DG models: stability of TR-BDF2

Setting $\mathbf{f}(\mathbf{y},t) = A\mathbf{y}(\mathbf{t})$, in eq. (1), then the stability function ϕ s.t. $\mathbf{u}^{n+1} = \phi(\Delta t A)\mathbf{u}^n$, if $\lambda = \alpha + i\omega \in eig(A)$, plotted in the $\alpha\Delta t - \omega\Delta t$ plane is:

TR-BDF2 off=0.0

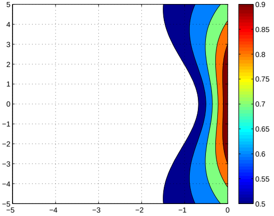

TR-BDF2 off=0.2

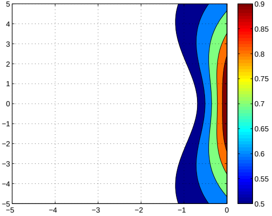

Crank Nicolson (CN) off=0.1

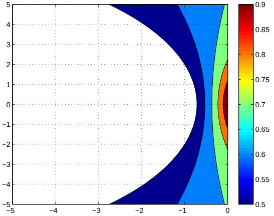

TR-BDF2 vs CN

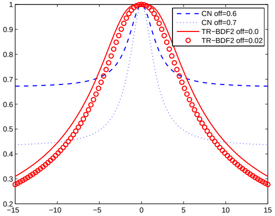

Time integrators for NWP-DG models: SL-TR-BDF2

Governing equations in advective form are to be solved ($\frac{D}{Dt}$ = Lagrangian derivative):

(SWE) Shallow Water Eqs. (no Coriolis force):

$$\frac{Dh}{Dt} + h\boldsymbol{\nabla}\cdot\mathbf{u} = 0,$$

$$\frac{D\mathbf{u}}{Dt} + g\boldsymbol{\nabla}h = -g\boldsymbol{\nabla}b,$$

with $h, \mathbf{u} = (u, v)^T$ and b being fluid depth, horizontal velocity and bathymetry elevation respectively,

(VSE) Euler eqs. (no Coriolis force) on a Vertical Slice ($\frac{\partial}{\partial y} = 0$):

$$\frac{D\Pi}{Dt} + \left(\frac{c_p}{c_v} - 1\right)\Pi\boldsymbol{\nabla}\cdot\mathbf{u} = 0,$$
$$\frac{Du}{Dt} + c_p\Theta\frac{\partial\pi}{\partial x} = 0,$$
$$\frac{Dw}{Dt} + c_p\Theta\frac{\partial\pi}{\partial z} - g\frac{\theta}{\theta^*} = 0,$$
$$\frac{D\theta}{Dt} + w\frac{d\theta^*}{dz} = 0.$$

with $\Theta = T\left(\frac{p}{p_0}\right)^{-R/c_p}, \Pi = \left(\frac{p}{p_0}\right)^{R/c_p}$, $p, T, \mathbf{u} = (u, w)^T$, pressure, temperature and vertical velocity, c_p, c_v, R specific heats and gas constant of dry air, and

$$\Pi(x, y, z, t) = \pi^*(z) + \pi(x, y, z, t),$$
$$\Theta(x, y, z, t) = \theta^*(z) + \theta(x, y, z, t),$$

where $\quad c_p\theta^*\frac{d\pi^*}{dz} = -g,$

Time integrators for NWP-DG models: SL technique

Given a velocity field $\mathbf{u}$, the Lagrangian derivative of a function f of space and time

$$\frac{Df}{Dt} = \lim_{\Delta t \to 0} \frac{f(\mathbf{X}(t+\Delta t), t+\Delta t) - f(\mathbf{X}(t), t)}{\Delta t}, \qquad \frac{d\mathbf{X}}{dt} = \mathbf{u}(\mathbf{X}(t), t)$$

is discretized as finite difference:

$$\begin{aligned} \frac{Df}{Dt} &\approx \frac{f(\mathbf{X}(t^{n+1}), t^{n+1}) - f(\mathbf{X}(t^n), t^n)}{\Delta t} \\ &\approx \frac{f(\mathbf{x}, t^{n+1}) - f(\mathbf{x}_D, t^n)}{\Delta t} \\ &\approx \frac{f^{n+1}(\mathbf{x}) - \left[E(t^n, \Delta t) f\right](\mathbf{x})}{\Delta t} \end{aligned}$$

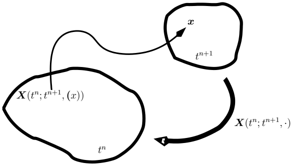

where $\mathbf{X}(t; t^{n+1}, \mathbf{x})$ is the the trajectory arriving in $\mathbf{x}$ at t^{n+1}:

$$\begin{cases} \frac{d}{dt}\mathbf{X}(t; t^{n+1}, \mathbf{x}) = \mathbf{u}^n\left(\mathbf{X}(t; t^{n+1}, \mathbf{x})\right) \\ \mathbf{X}(t^{n+1}; t^{n+1}, \mathbf{x}) = \mathbf{x} \end{cases},$$

and $\mathbf{x}_D = \mathbf{X}(t^n; t^n, \mathbf{x}) = \mathbf{x} - \int_{t^n}^{t^{n+1}} \mathbf{u}^n\left(\mathbf{X}(t; t^{n+1}, \mathbf{x})\right) dt$ is the departure point of $\mathbf{x}$.

The action of the SL evolution operator $[E(t^n, \Delta t) f](\mathbf{x}) = f^n(\mathbf{x}_D)$ consists then in:

1. departure point $\mathbf{x}_D$ computation;
2. interpolation of f^n at departure point;

Time integrators for NWP-DG models: SL-TR

... then SISL-TR steps for SWE and VSE are isomorphic

$$h^{n+2\gamma} + \gamma\Delta t \; h^n \; \boldsymbol{\nabla}\cdot\mathbf{u}^{n+2\gamma} =$$
$$E\left(t^n, 2\gamma\Delta t\right)\left[h - \gamma\Delta t \; h \; \boldsymbol{\nabla}\cdot\mathbf{u}\right],$$

$$\mathbf{u}^{n+2\gamma} + \gamma\Delta t \; g\boldsymbol{\nabla}h^{n+2\gamma} = -\gamma\Delta t \; g\boldsymbol{\nabla}b$$
$$+ E\left(t^n, 2\gamma\Delta t\right)\left\{\mathbf{u} - \gamma\Delta t\left[g(\boldsymbol{\nabla}h + \boldsymbol{\nabla}b)\right]\right\}.$$

$$\pi^{n+2\gamma} + \gamma\Delta t \; \left(c_p/c_v - 1\right)\Pi^n \boldsymbol{\nabla}\cdot\mathbf{u}^{n+2\gamma} = -\pi^*$$
$$+ E\left(t^n, 2\gamma\Delta t\right)\left[\Pi - \gamma\Delta t\left(c_p/c_v - 1\right)\Pi \; \boldsymbol{\nabla}\cdot\mathbf{u}\right],$$

$$u^{n+2\gamma} + \gamma\Delta t \; c_p\Theta^n \frac{\partial\pi}{\partial x}^{n+2\gamma} =$$
$$E(t^n, 2\gamma\Delta t)\left[u - \gamma\Delta t \; c_p\Theta\frac{\partial\pi}{\partial x}\right],$$

$$\left(1 + (\gamma\Delta t)^2\frac{g}{\theta^*}\frac{d\theta^*}{dz}\right)w^{n+2\gamma} + \gamma\Delta t c_p\Theta^n\frac{\partial\pi}{\partial z}^{n+2\gamma} =$$
$$E(t^n, 2\gamma\Delta t)\left[w - \gamma\Delta t\left(c_p\Theta\frac{\partial\pi}{\partial z} - g\frac{\theta}{\theta^*}\right)\right]$$
$$+ \gamma\Delta t\frac{g}{\theta^*}E(t^n, 2\gamma\Delta t)\left[\theta - \gamma\Delta t\frac{d\theta^*}{dz}w\right].$$

$$h \longleftrightarrow \pi,$$
$$u \longleftrightarrow u,$$
$$v \longleftrightarrow w.$$

Time integrators for NWP-DG models: SL-BDF2

and SISL-BDF2 steps for SWE and VSE are isomorphic:

$$h^{n+1} + \gamma_2 \Delta t \; h^{n+2\gamma} \; \boldsymbol{\nabla} \cdot \mathbf{u}^{n+1} =$$
$$\left(1-\gamma_3\right) E(t^n, \Delta t) h$$
$$+ \gamma_3 E(t^n + 2\gamma\Delta t, (1-2\gamma)\Delta t) h,$$

$$\mathbf{u}^{n+1} + \gamma_2 \Delta t \; g \boldsymbol{\nabla} h^{n+1} =$$
$$- \gamma_2 \Delta t \; g \boldsymbol{\nabla} b$$
$$+ \left(1-\gamma_3\right) E(t^n, \Delta t) \mathbf{u}$$
$$+ \gamma_3 E(t^n + 2\gamma\Delta t, (1-2\gamma)\Delta t) \mathbf{u}.$$

$$\pi^{n+1} + \gamma_2 \Delta t \left(c_p/c_v - 1\right) \Pi^{n+2\gamma} \boldsymbol{\nabla} \cdot \mathbf{u}^{n+1} =$$
$$- \pi^* + (1-\gamma_3)[E(t^n, \Delta t)\Pi]$$
$$+ \gamma_3 [E(t^n + 2\gamma\Delta t, (1-2\gamma)\Delta t)\Pi],$$

$$u^{n+1} + \gamma_2 \Delta t \; c_p \Theta^{n+2\gamma} \frac{\partial \pi}{\partial x}^{n+1} =$$
$$(1-\gamma_3)[E(t^n, \Delta t) u]$$
$$+ \gamma_3 [E(t^n + 2\gamma\Delta t, (1-2\gamma)\Delta t) u],$$

$$\left(1 + (\gamma_2 \Delta t)^2 \frac{g}{\theta^*} \frac{d\theta^*}{dz}\right) w^{n+1} + \gamma_2 \Delta t \; c_p \Theta^{n+2\gamma} \frac{\partial \pi}{\partial z}^{n+1} =$$
$$(1-\gamma_3)[E\left(t^n, \Delta t\right) w] + \gamma_3 [E(t^n + 2\gamma\Delta t, (1-2\gamma)\Delta t) w] +$$
$$\gamma_2 \Delta t \frac{g}{\theta^*} \left\{(1-\gamma_3)[E(t^n, \Delta t)\theta] + \gamma_3 [E(t^n + 2\gamma\Delta t, (1-2\gamma)\Delta t)\theta]\right\}$$

$$\begin{aligned} h &\longleftrightarrow \pi, \\ u &\longleftrightarrow u, \\ v &\longleftrightarrow w. \end{aligned}$$

Time integrators for NWP-DG models: mass conservative SISL-TR-BDF2

Considering the continuity equation in Eulerian flux form, while the momentum one in advective vector form:

$$\frac{\partial \eta}{\partial t} = -\boldsymbol{\nabla} \cdot (h\mathbf{u}),$$
$$\frac{D\mathbf{u}}{Dt} = -g\boldsymbol{\nabla}\eta - f\mathbf{k} \times \mathbf{u},$$

then, the TR stage of the SISL time discretization of previous equations is:

$$\eta^{n+2\gamma} + \gamma\Delta t\, \boldsymbol{\nabla} \cdot \left(h^n \mathbf{u}^{n+2\gamma}\right) = \eta^n - \gamma\Delta t\, \boldsymbol{\nabla} \cdot (h^n \mathbf{u}^n),$$

$$\mathbf{u}^{n+2\gamma} + \gamma\Delta t \left(g\boldsymbol{\nabla}\eta^{n+2\gamma} + f\mathbf{k} \times \mathbf{u}^{n+2\gamma}\right)$$
$$= E\left(t^n, 2\gamma\Delta t\right) \left[\mathbf{u} - \gamma\Delta t \left(g\boldsymbol{\nabla}\eta + f\mathbf{k} \times \mathbf{u}\right)\right].$$

The TR stage is then followed by the BDF2 stage:

$$\eta^{n+1} + \gamma_2\Delta t\, \boldsymbol{\nabla} \cdot \left(h^{n+2\gamma}\mathbf{u}^{n+1}\right) = \left(1 - \gamma_3\right)\eta^n + \gamma_3\, \eta^{n+2\gamma},$$

$$\mathbf{u}^{n+1} + \gamma_2\Delta t \left(g\boldsymbol{\nabla}\eta^{n+1} + f\mathbf{k} \times \mathbf{u}^{n+1}\right)$$
$$= \left(1 - \gamma_3\right) E\left(t^n, \Delta t\right)\mathbf{u} + \gamma_3 E\left(t^n + 2\gamma\Delta t, (1 - 2\gamma)\Delta t\right)\mathbf{u}.$$

Choice of basis functions: DG space discretization

- Defined a tassellation $\mathcal{T}_h = \{K_I\}_{I=1}^{N}$ of domain Ω and chosen $\forall K_I \in \mathcal{T}_h$ three integers $p_I^{\pi} \geq 0$, $p_I^{\theta} \geq 0$, $p_I^{u} \geq 0$, at each time level t^n, we are looking for approximate solution s.t.

$$\begin{aligned} h^n, \pi^n &\in P_h := \left\{ f \in L^2(\Omega) \; : \; f|_{K_I} \in \mathbb{Q}_{p_I^{\pi}}(K_I) \right\} \\ \theta^n &\in T_h := \left\{ f \in L^2(\Omega) \; : \; f|_{K_I} \in \mathbb{Q}_{p_I^{\theta}}(K_I) \right\} \\ u^n, v^n, w^n &\in V_h := \left\{ g \in L^2(\Omega) \; : \; g|_{K_I} \in \mathbb{Q}_{p_I^{u}}(K_I) \right\}, \end{aligned}$$

- modal bases are used to span P_h, T_h, V_h,
- L^2 projection against test functions (chosen equal to the basis functions),
- introduction of *centered* numerical fluxes,
- substitution of velocity d.o.f. from momentum eqs. into the continuity eq., (Schur complement form)
- give raise, at each SI step, to a discrete (vector) Helmholtz equation in the fluid depth / pressure unknown only,

i.e. a sparse block structured nonsymmetric linear system is solved by GMRES with *block* diagonal (for the moment) preconditioning.

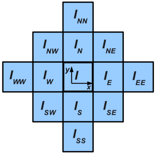

Choice of adaptativity strategy: dynamic p-adaptation

- being a model variable α represented in element K_I as:

$$\alpha_{|K_I} = \sum_{k=1}^{p^{\alpha}_{I,1}+1} \sum_{l=1}^{p^{\alpha}_{I,2}+1} \sum_{m=1}^{p^{\alpha}_{I,3}+1} \alpha_{I,k,l,m}\, \psi_k \psi_l \psi_m .$$

- and its 2-norm given by (in Cartesian geometry):

$$\mathcal{E}_I = \sum_{k=1}^{p^{\alpha}_{I,1}+1} \sum_{l=1}^{p^{\alpha}_{I,2}+1} \sum_{m=1}^{p^{\alpha}_{I,3}+1} \alpha^2_{I,k,l,m}$$

$$= \sum_{r=1}^{\max_d p^{\alpha}_{I,d}+1} \mathcal{E}^r_I, \quad \text{where} \quad \mathcal{E}^r_I := \sum_{\max(k,l,m)=r} \alpha^2_{I,k,l,m},$$

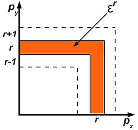

- while the quantity $w^r_I = \sqrt{\frac{\mathcal{E}^r_I}{\mathcal{E}_I}}$ measuring the relative 'weight' of the $r-$ degree modes
- *Given an error tolerance $\epsilon_I > 0$ for all $I = 1, \ldots, N$, at each time step repeat following steps:*

1) *compute w^r_I for $r = max_d p^{\alpha}_{I,d} + 1, \ldots, 1$*

2.1) *if $w^r_I \geq \epsilon_I$, then*

   2.1.1) *set $p^{\alpha}_{I,d} := min(r+1, pmax_{I,d})$*

   2.1.2) *set $\alpha_{I,p_{I,1},p_{I,2},p_{I,3}} = 0$, exit the loop and go the next element*

2.2) *if instead $w^r_I < \epsilon_I$, then*

   2.2.1) *compute w^{r-1}_I*

   2.2.2) *if $w^{r-1}_I \geq \epsilon_I$, exit the loop go to 2.1.1 and then go the next element*

   2.2.3) *else if $w^{r-1}_I < \epsilon_I$, set $p^{\alpha}_{I,d} := p^{\alpha}_{I,d} - 1, \quad d = 1, \ldots, 3$ and go back to 2.2.1.*

Choice of adaptativity strategy for NWP: potential of $p-$adaptivity

- No remeshing required of many physical quantities like orography profiles, data on land use and soil type, land-sea masks.

- Completely independent resolution for each single model variable.

- Easier coupling with SL technique, especially on unstructured meshes (no need to store two meshes).

- use of static p-adaptation with independent polynomial degree in the three directions and in each element:
  - reduced p as counterpart of reduced grid to control the local Courant number near poles ($\Longrightarrow$ significant #gmres-iterations reduction).
  - more uniform the resolution by $p_{I,z} < p_{I,x}, p_{I,y}$, considering the aspect ratio of the mesh elements (the atmosphere is thin);

- Main potential problem: dynamic load balancing is mandatory for massively parallel implementations.

choice of mesh: mesh deformation on the sphere

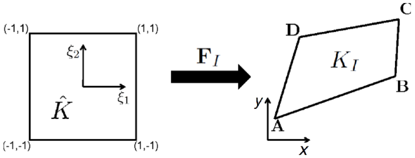

$$x = F_{I,1}(\xi_1, \xi_2) = x_I^A \frac{1-\xi_1}{2} \frac{1-\xi_2}{2} + x_I^B \frac{1+\xi_1}{2} \frac{1-\xi_2}{2} + x_I^C \frac{1+\xi_1}{2} \frac{1+\xi_2}{2} + x_I^D \frac{1-\xi_1}{2} \frac{1+\xi_2}{2},$$

$$y = F_{I,2}(\xi_1, \xi_2) = y_I^A \frac{1-\xi_1}{2} \frac{1-\xi_2}{2} + y_I^B \frac{1+\xi_1}{2} \frac{1-\xi_2}{2} + y_I^C \frac{1+\xi_1}{2} \frac{1+\xi_2}{2} + y_I^D \frac{1-\xi_1}{2} \frac{1+\xi_2}{2},$$

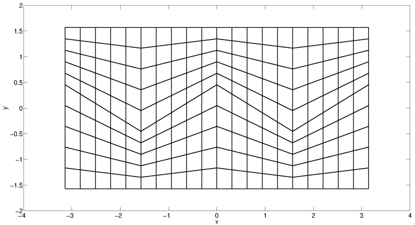

example adapted from Weller 2012 to mimick cubed sphere mesh distortion

choice of mesh: unstructured meshes capability

- we can use *unstructured meshes of hexaedra*:

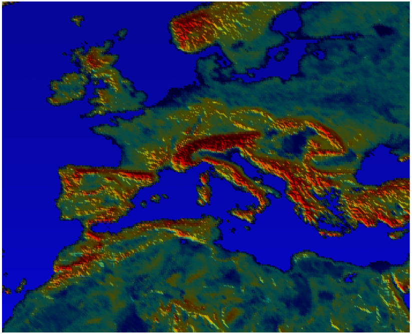

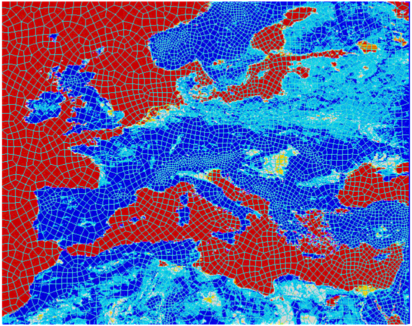

- for geophysical applications (for both atmosphere and ocean):
  - a 2-D unstructured mesh of quads is constructed with $h-$ refinement according to the slope of the orography;
  - then it is extruded along the vertical direction;
  - the bottom is shifted so as to follow the orography profile;
- $[-1,1]^3$ is mapped onto each mesh element by a *trilinear map*: curved faces hexaedral elements are supported.

other choices for the mesh:

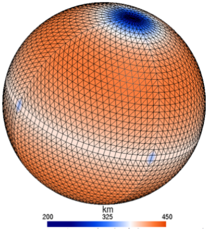

Figure: Octahedral mesh

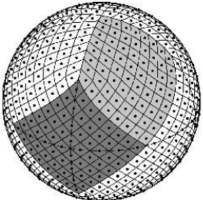

Figure: Healpix mesh

Healpix mesh - Hierarchical Equal Area isoLatitude Pixelation of a sphere as a quad counterpart of the reduced octahedral mesh currently under investigation by W. Deconinck and S. Bradar at ECMWF:

- to reduce the number of grid points towards the poles;
- to improve intercomparison with other approaches, e.g. spectral transform, FVM;
- to improve the coupling with physical parametrizations.

choioce of vertical coordinate: mesh deformation on a vertical plane

Orography in z coordinate: this is the natural extension of DG approach from CFD;

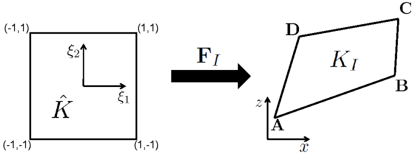

$$x = F_{I,1}(\xi_1, \xi_2) = x_I^A \frac{1-\xi_1}{2}\frac{1-\xi_2}{2} + x_I^B \frac{1+\xi_1}{2}\frac{1-\xi_2}{2} + x_I^C \frac{1+\xi_1}{2}\frac{1+\xi_2}{2} + x_I^D \frac{1-\xi_1}{2}\frac{1+\xi_2}{2},$$

$$z = F_{I,2}(\xi_1, \xi_2) = z_I^A \frac{1-\xi_1}{2}\frac{1-\xi_2}{2} + z_I^B \frac{1+\xi_1}{2}\frac{1-\xi_2}{2} + z_I^C \frac{1+\xi_1}{2}\frac{1+\xi_2}{2} + z_I^D \frac{1-\xi_1}{2}\frac{1+\xi_2}{2}.$$

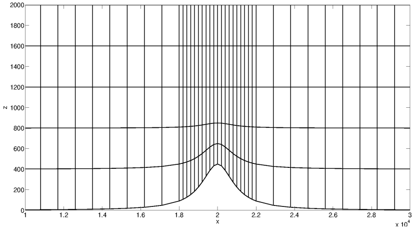

choice of vertical coordinate: terrain following vertical coordinate

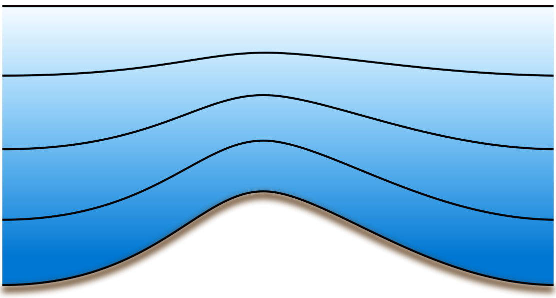

- better representation of PBL;
- easier implementation of BC (especially for the SL step with steep orography);
- easier coupling with physics;
- already successfully combined with DG at DWD;
- pressure based option also under evaluation.

choice of data structures

- Tensor products of 1-D Legendre polynomials: direct addressing of dofs within hexaedral elements;
- direct addressing of elemental quadrature nodes and weights, whose number is adapted in each direction according to the local polynomial degree;
- elements organized by columns, i.e. indirect addressing in horizontal, direct addressing in the vertical:
  - 2-D horizontal mesh extruded in vertical columns;
  - better access to memory;
  - better coupling with physics;
- use of global arrays of pointers to local columnwise data structures;
- example of these data structures as well as DG operators on the sphere relevant for SI and SL techniques (grad, div, Laplacian) have been implemented in a parallel and p-adaptive 3-D DG libary called Panther:

P

Adaptive

Numerical

Tool for

High order

Efficient disc**R**etizations

choice of parallelization: challenges from a p-SISL-DG model

- Communication overhead due to large stencil for SI time discretization approach:

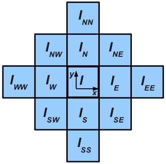

- communication overhead due to large stencil for SL time discretization approach:

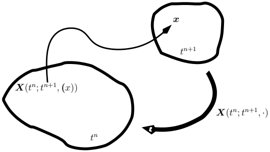

- smart dynamic load balancing required to guarantee scalability of dynamically adaptive approaches:

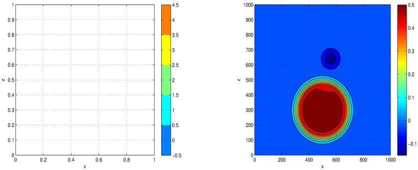

choice of parallelization

- horizontal domain decomposition (columnwise approach);
- one sided communications, different approaches available. e.g. MPI3 or Fortran coarrays (PGAS model);
- shared memory parallelisation (multi-threading) with OpenMP within a node;
- communication on demand for the semi-Lagrangian step;
- two elements deep stencil can allow for high Courant numbers with high order DG;
- GPU implementation envisaged, relying on Atlas' accelerator aware data structures;
- use of *indirect* addressing for the columns useful also for implementation of effective column migration strategies (e.g. by following space filling curves);

Numerical Validation

Shallow Water Equations (SWE) on the sphere

Unsteady flow with analytic solution (Läuter 2005): TR-BDF2 vs off centerd Crank Nicolson

- Relative errors for TR-BDF2 at different resolutions, Δt in seconds:

$N_x \times N_y$	Δt	$l_1(h)$	$l_2(h)$	$l_\infty(h)$	q_2^{emp}
10×5	3600	5.46×10^{-3}	6.12×10^{-3}	9.54×10^{-3}	-
20×10	1800	1.25×10^{-3}	1.40×10^{-3}	2.14×10^{-3}	2.1
40×20	900	3.04×10^{-4}	3.41×10^{-4}	5.21×10^{-4}	2.0
80×40	450	7.55×10^{-5}	8.47×10^{-5}	1.29×10^{-4}	2.0

- Relative errors for off-centered Crank Nicolson ($\theta = 0.6$) at different resolutions:

$N_x \times N_y$	Δt	$l_1(h)$	$l_2(h)$	$l_\infty(h)$	q_2^{emp}
10×5	3600	1.44×10^{-2}	1.63×10^{-2}	2.40×10^{-2}	-
20×10	1800	8.74×10^{-3}	9.89×10^{-3}	1.44×10^{-2}	0.7
40×20	900	4.81×10^{-3}	5.45×10^{-3}	7.96×10^{-3}	0.9
80×40	450	2.53×10^{-3}	2.86×10^{-3}	4.18×10^{-3}	0.9

- At max. resolution in space and time (80×40 el., $\Delta t = 450$s) error norms for TR-BDF2 are around 34 times smaller than those of off-centered Crank Nicolson, while CPU time is equivalent (104.3s for a time step of TR-BDF2 vs 99.9s for a time step of off centerd CN).

- At fixed resolution in space (40×20 el.), off centered Crank Nicolson needs to be run with a 16 times smaller Δt in order to reach same level of accuracy of TR-BDF2 with $\Delta t = 900$s. $\Longrightarrow$ CPU time for TR-BDF2 is around 20% that of off-centered CN for same accuracy.

Williamson’s test 6: static + dynamic p-adaptation combined

64×32 elements, $\max p^h = 4$, $\Delta t = 900s$ ($C_{cel} \approx 83$ without adaptivity).

$$\frac{\#\text{gmres-iterations}(p^h = \text{adapted})}{\#\text{gmres-iterations}(p^h = \text{uniform})} \approx 13\%, \qquad \Delta^n_{dof} = \frac{\sum_{I=1}^{N} (p^n_I + 1)^2}{N(p_{max} + 1)^2} \approx 45\%.$$

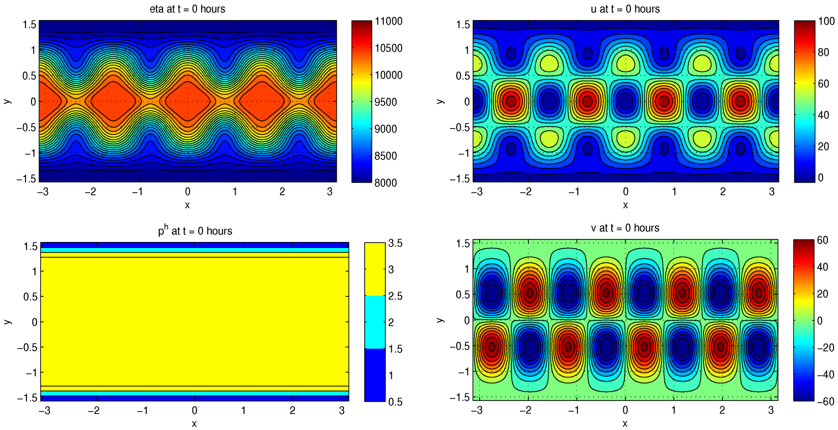

Williamson's test 6: time convergence rate and p-adaptation efficiency

- Relative errors at $t_f = 15$ days for different number of elements, with respect to NCAR spectral model solution at resolution T511:

$N_x \times N_y$	Δt[min]	$l_1(h)$	$l_2(h)$	$l_\infty(h)$	q_2^{emp}
10×5	60	2.92×10^{-2}	3.82×10^{-2}	6.75×10^{-2}	-
20×10	30	5.50×10^{-3}	6.80×10^{-3}	1.11×10^{-2}	2.4
40×20	15	1.40×10^{-3}	1.80×10^{-3}	3.20×10^{-3}	2.0

- Relative differences btw adaptive (tol. $\epsilon = 10^{-2}$) and nonadaptive solution at $t_f = 15$ days:

adaptivity	$l_1(h)$	$l_2(h)$	$l_\infty(h)$
static	2.182×10^{-4}	3.434×10^{-4}	2.856×10^{-4}
static + dynamic	3.407×10^{-4}	4.301×10^{-4}	7.484×10^{-4}

- CPU time: static and dynamic p-adaptive solution execution time is around 24% of that for nonadaptive solution.

Williamson's test 6: deformed vs. aligned mesh

$p^{\eta} = 4, \quad p^{u} = 5, \quad N_x \times N_y = 32 \times 16, \qquad t_f = 15$days

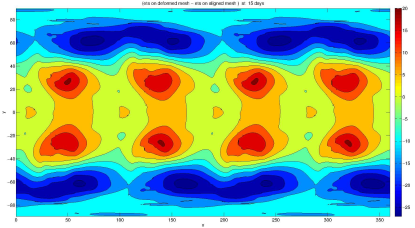

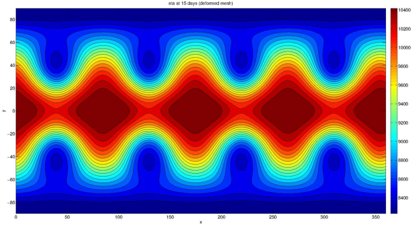

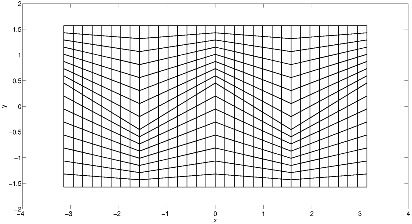

$$d_i = \|\eta_{def} - \eta_{alg}\|_i, i = 1, 2, \inf$$

$$d_1 = 1.058 \times 10^{-3}$$

$$d_2 = 1.263 \times 10^{-3}$$

$$d_\infty = 2.568 \times 10^{-3}$$

Stommel gyre: dynamic adaptation

Two months simulation, max $p = 4, C_{cel} \approx 24$, computational cost reduction $\approx 50\%$

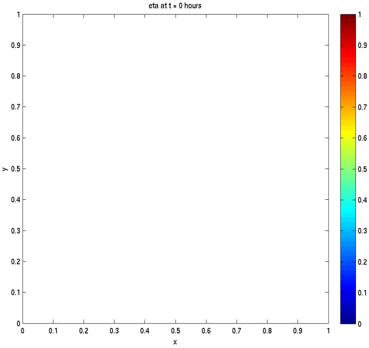

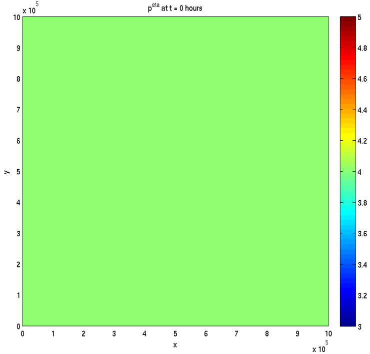

p-adaptive tracers advection

Recap: the power of SL-DG

The combination SL-DG can be very efficient, especially if many-tracers (hundreds of them) transport is envisaged, because:

- for each quadrature node, departure point is computed just once and for all the transported variables, no matter how many they are;
- at each departure point, modal basis functions are evaluated just once (as they are hierachical) and for all the transported variables, no matter how many these are;
- expansion over basis functions at departure point contains different number of terms for each transported field according to its 'private' local degree (resolution).

Solid body rotation on the sphere

120×60 elements, max $p^c = 4$, $\Delta t =$ 7200s, $C_{vel,x} \approx$ 400, $C_{vel,y} \approx$ 4

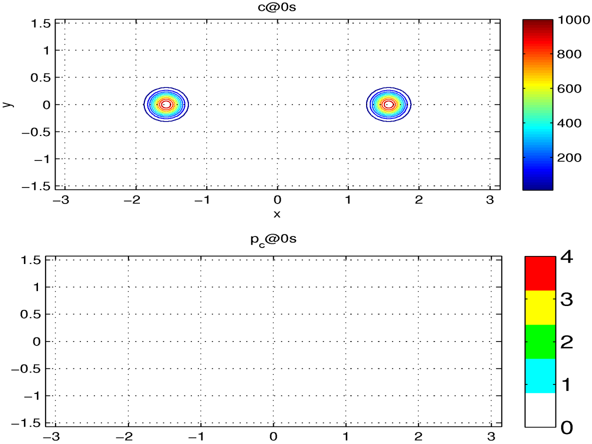

Deformational flow on the sphere (adapted from Nair, Lauritzen 2010)

80×40 elements, max $p^c = 4$, $\Delta t = 1800$s

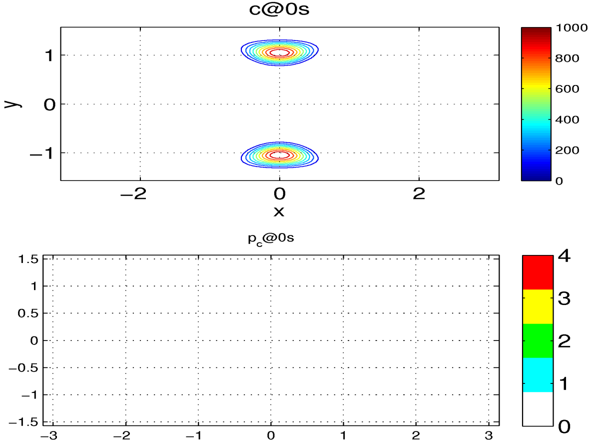

Rossby Haurwitz wave velocity field

120×60 elements, max $p^c = 4$, $\Delta t = 900s$, $C_{vel,x} \approx 1$

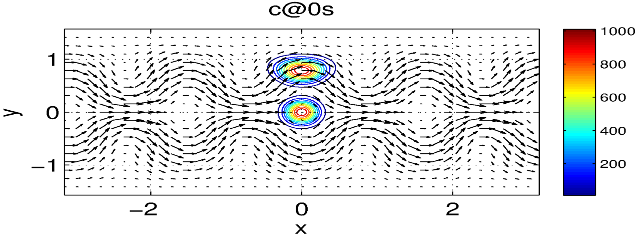

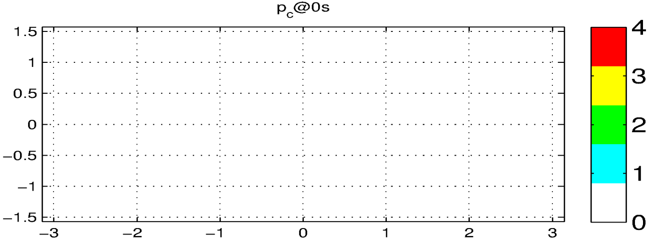

Hadley cell like motion, DCMIP 1-2

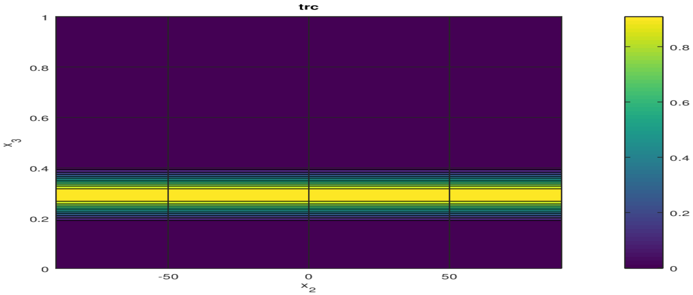

1/2 deg, 60 lev, $\Delta t = 1920$s, final $||err||_1 \approx 1.16e-2$, $||err||_2 \approx 1.2e-2$,
Δt 13 times longer than the maximum allowed for RK-DG (RK4), in addition SL-DG exhibits a smaller error.

Nonlinear advection: Burgers equation

- Flux-form SL-DG (similar approach to Restelli at al. JCP 2006);
- Courant number $C = 7.2$;
- Black line represents the initial sinusoidal profile, while red line is the solution computed at $t = 0.3s$ i.e. near the shock formation time.

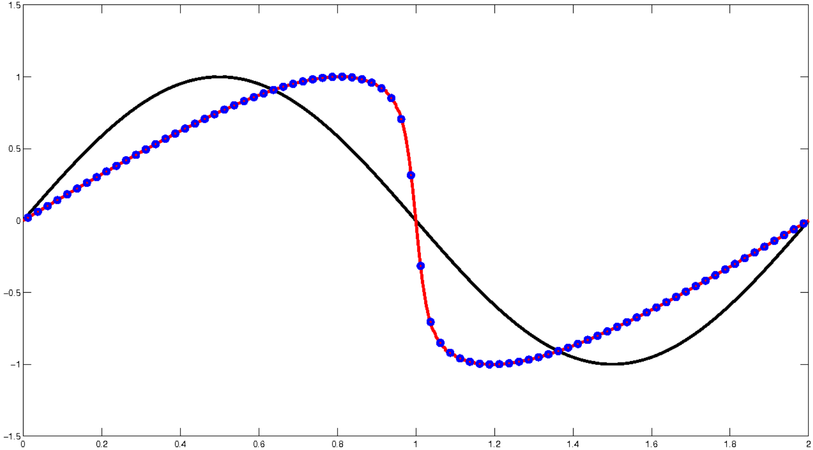

Euler equations on a Vertical Slice (VSE)

Warm bubble test (Carpenter et al., MWR 1990)

49×60 elements, $p^{\pi} = 4$, $p^{u} = 5$, $\Delta t = 1$ s, $C \approx 18$.

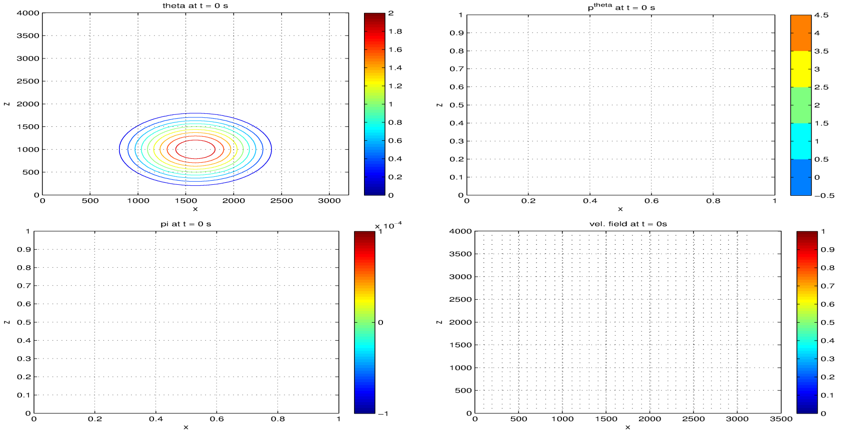

variable	l_1	l_2	l_∞
π	2.744×10^{-3}	4.92×10^{-3}	3.86×10^{-2}
θ	1.70×10^{-2}	4.38×10^{-2}	9.34×10^{-2}
u	3.64×10^{-4}	1.14×10^{-3}	3.60×10^{-2}

Table: Relative differences between adaptive and nonadaptive solution for warm bubble test case.

Interacting bubbles test (Robert, 1993)

50×50 elements, $p^{\pi} = 4,\ p^{u} = 5, \quad \Delta t = 1$ s, $C \approx 87.$

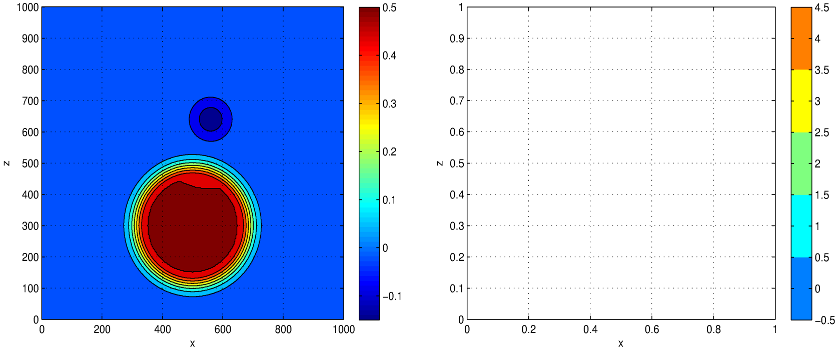

Inertia-gravity wave (Skamarock and Klemp, MWR 1994)

300×10 elements, $p^{\pi} = 4$, $p^{u} = 5$, $\Delta t = 15$ s, $C \approx 25$.

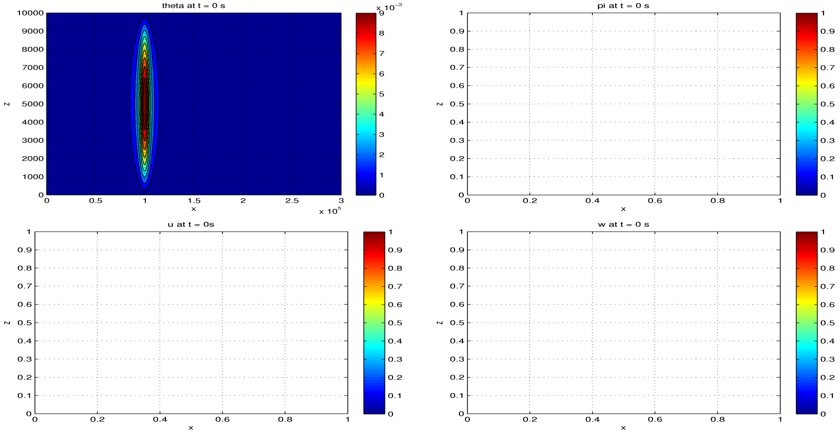

$N_x \times N_y$	Δt	$l_1(\theta)$	$l_2(\theta)$	$l_\infty(\theta)$	q_2^{emp}
60×2	8	5.33×10^{-2}	3.44×10^{-2}	1.22×10^{-2}	-
120×4	4	1.29×10^{-2}	7.89×10^{-3}	4.03×10^{-3}	2.1
240×8	2	2.58×10^{-3}	1.56×10^{-3}	1.36×10^{-3}	2.3

Linear hydrostatic lee waves

60×50 elements, $p^{\pi} = 4,\ p^{u} = 5,\quad \Delta t = 7$ s, $C_V \approx 7, C_H \approx 9.$

(maximum space resolution 2 km)

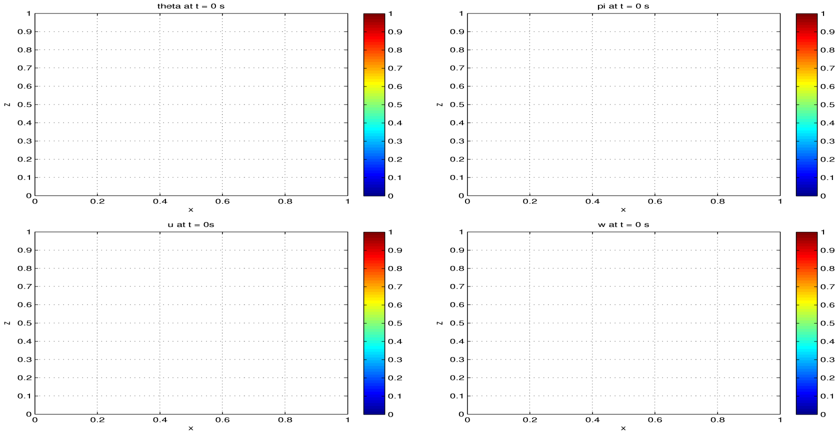

Linear hydrostatic lee waves: adaptive run

60×50 elements, $p^{\pi} = p^{u} = 4$, $\Delta t = 7$ s, $C_V \approx 7, C_H \approx 9$.

(maximum space resolution 2 km)

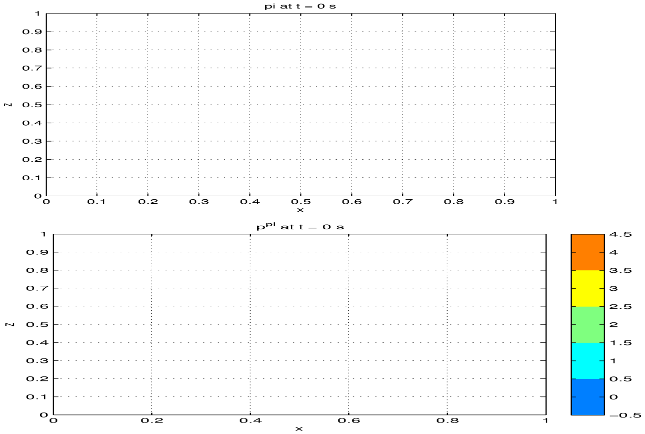

Nonlinear nonhydrostatic lee waves

60×50 elements, $p^{\pi} = 4,\ p^{u} = 5,\quad \Delta t = 2$ s, $C_V \approx 25, C_H \approx 13.$

(maximum space resolution 200m)

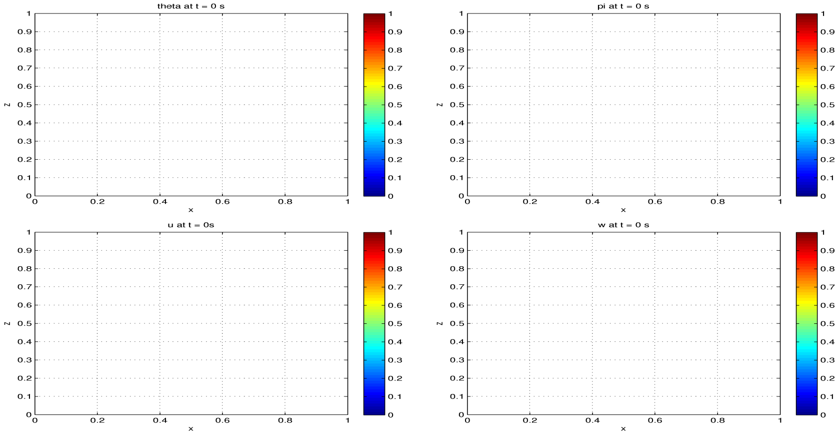

Nonlinear nonhydrostatic lee waves: adaptive run

100×50 elements, $p^{\pi} = p^{u} = 4$, $\Delta t = 2$ s, $C_V \approx 25, C_H \approx 13.$

(maximum space resolution 200m)

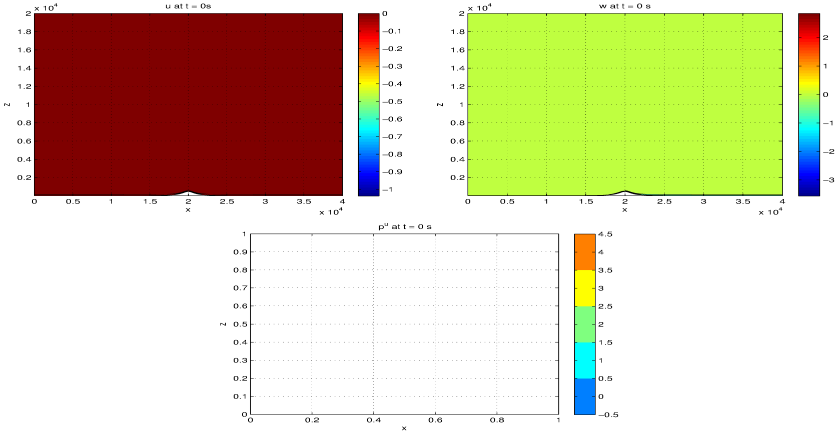

- DG methods definitely promising for NWP, for example the novel SISL-DG discretization presented for the rotating SWE as well as for the Euler equations, can be effectively applied to NWP as it exhibits:
  - unconditional stability,
  - full second order accuracy in time,
  - arbitrary high order accuracy in space,
  - adaptation of the number of degrees of freedom in each element to balance accuracy and computational cost,
  - equipped with Schur complement form;
  - compliant with deformed as well as to arbitrary non-structured even non-conforming meshes,
  - amenable to mass conservative versions;
- to fully exploit the DG potential for NWP, a lot of work required in many related topics including:
  - time integrators;
  - data structures and code design;
  - parallel HPC programming;
  - mesh generation;
- each of the previous topic requires choices to be specifically made for NWP.

- DG methods definitely promising for NWP, for example the novel SISL-DG discretization presented for the rotating SWE as well as for the Euler equations, can be effectively applied to NWP as it exhibits:
  - unconditional stability,
  - full second order accuracy in time,
  - arbitrary high order accuracy in space,
  - adaptation of the number of degrees of freedom in each element to balance accuracy and computational cost,
  - equipped with Schur complement form;
  - compliant with deformed as well as to arbitrary non-structured even non-conforming meshes,
  - amenable to mass conservative versions;
- to fully exploit the DG potential for NWP, a lot of work required in many related topics including:
  - time integrators;
  - data structures and code design;
  - parallel HPC programming;
  - mesh generation;
- each of the previous topic requires choices to be specifically made for NWP.
- THANK YOU FOR YOUR ATTENTION!

References

- Tumolo G., Bonaventura L., and Restelli M. 2013. A semi-implicit, semi-Lagrangian, p-adaptive discontinuous Galerkin method for the shallow water equations. *Journal of Computational Physics.* Vol. 232, pp. 46-67

- Tumolo G., Bonaventura L. 2015. A semi-implicit, semi-Lagrangian discontinuous Galerkin framework for adaptive numerical weather prediction. *Quarterly Journal of the Royal Meteorological Society.* Vol. 141, pp. 2582-2601.

- Tumolo G. 2016. A mass conservative TR-BDF2 semi-implicit semi-Lagrangian DG discretization of the shallow water equations on general structured meshes of quadrilaterals. *Communications in Applied and Industrial Mathematics,* 7(3), pp. 165-190.

- Tumolo G., Bonaventura L. 2020. Simulations of Non-hydrostatic Flows by an Efficient and Accurate p-Adaptive DG Method. *In: van Brummelen H., Corsini A., Perotto S., Rozza G. (eds) Numerical Methods for Flows. Lecture Notes in Computational Science and Engineering*, vol 132. Springer, Cham. https://doi.org/10.1007/978-3-030-30705-9_5

- Tumolo G., Deconinck W., and Paronuzzi-Ticco. S.V. 2020. PANTHER: a p adaptive discontinuous Galerkin parallel library for effcient high order computations. In preparation

- Tumolo G. 2020. Parallel semi-Lagrangian discontinuous Galerkin advection. In preparation

- Tumolo G. 2020. Departure point approximations for high order Lagrange- Galerkin methods: accuracy and effciency assessment in a parallel framework. In preparation